Low-symmetry monoclinic ferroelectric phase stabilized by oxygen octahedra rotations in strained $Eu_xSr_{1-x}TiO_3$ thin films

Anna N. Morozovska,[1,2] Yijia Gu,[3] Victoria V. Khist,[2] Maya D. Glinchuk,[2] Long-Qing Chen,[3,*] Venkatraman Gopalan,[3,†] and Eugene A. Eliseev[2,‡]

[1]*Institute of Physics, NAS of Ukraine, 46, pr. Nauki, 03028 Kiev, Ukraine*

[2]*Institute for Problems of Materials Science, NAS of Ukraine, Krjijanovskogo 3, 03142 Kiev, Ukraine*

[3]*Department of Materials Science and Engineering, Pennsylvania State University, University Park, Pennsylvania 16802, USA*

(Received 3 January 2013; revised manuscript received 25 February 2013; published 10 April 2013)

Using Landau–Ginzburg–Devonshire theory and phase-field modeling, we explore the complex interplay between a structural order parameter (oxygen octahedron rotation) and polarization in $Eu_xSr_{1-x}TiO_3$ thin films. Under a biaxially tensile strain, a low-symmetry monoclinic phase with in-plane ferroelectric polarization is found to be stabilized by antiferrodistortive oxygen octahedra tilts. The monoclinic phase is stable over a wide temperature range. It is characterized by a large number of energetically equivalent polar and structural twin domains. This work demonstrates the development of a spontaneous polarization and piezo- and pyroelectricity in a ferroelastic twin boundary arising from flexoelectric coupling and rotostriction.

DOI: 10.1103/PhysRevB.87.134102 PACS number(s): 77.80.bn, 68.55.−a

I. INTRODUCTION

Epitaxial strains imposed on commensurate complex oxide thin films by substrates can lead to the emergence of a broad range of new properties[1] such as ferroelectricity,[2,3] magnetism,[4] octahedral tilts,[5] and multiferroicity[6] as well as new phases with strong polar or magnetic long-range order that are absent in the corresponding bulk ferroelastics and quantum paraelectrics.[1–5,7]

As a classical example, $SrTiO_3$ has been extensively studied during the last a few decades. Bulk $SrTiO_3$ is a nonmagnetic quantum paraelectric[8] with antiferrodistortive (AFD) structural order below 105 K.[9–11] However, strained $SrTiO_3$ films have been shown to possess a wide range of intriguing properties, including octahedral tilts and ferroelectricity at high temperature,[7,12,13] superconductivity,[14] and, surprisingly, magnetism,[15] whose origin remains uncertain.[16] Another similar material that is relatively new and actively studied is $EuTiO_3$. The bulk quantum paraelectric $EuTiO_3$ is a low-temperature antiferromagnet.[17,18] It exhibits an antiferrodistortion transition at 281 K[19–23] and is paraelectric at high temperatures. The strained $EuTiO_3$ films, surprisingly, become strong ferroelectric ferromagnets under epitaxial strains exceeding 1%.[24–26]

The main focus of this work is on much less studied strained films of quantum paraelectric $Eu_xSr_{1-x}TiO_3$. Since $Eu_xSr_{1-x}TiO_3$ films are solid solutions of $EuTiO_3$ and $SrTiO_3$, they may exhibit not only all the interesting structural and polar mode interactions of individual $EuTiO_3$ and $SrTiO_3$ films but also new phenomena and properties. There has been one experimental study on the structural AFD and other physical properties of bulk solid solution $Eu_xSr_{1-x}TiO_3$.[27] Theoretically, possible multiferroic properties of $Eu_xSr_{1-x}TiO_3$ nanotubes and nanowires[28] have been predicted using Landau–Ginzburg–Devonshire (LGD) theory. However, in Ref. 28 the structural AFD order parameter was considered as a scalar, while the true AFD order parameter is an axial vector describing the oxygen octahedral tilt.[29] The vector nature of the AFD order parameter can strongly influence the phase stability and polar and pyroelectric properties of quantum paraelectrics[11,30] at interfaces[31] or in thin film bulk.[7,13,32]

Phase diagrams of strained films are usually complicated by new phases, which are absent in their bulk counterparts. Among these emergent new phases, low-symmetry monoclinic phases are of particular interest due to the relative large number of possible ferroelectric and ferroelastic twin variants and wall orientations compared to higher symmetry phases, which give rise to possible dramatic enhancements in piezoelectric coefficients. Monoclinic phases with in-plane and out-of-plane polarization components of different amplitudes have been predicted theoretically in epitaxial $BaTiO_3$ films.[33–35] In the strained incipient ferroelectric $SrTiO_3$ films, only tetragonal and orthorhombic phases were shown to be stable.[7,13] However, the addition of Eu to $SrTiO_3$ thin films may result in the stabilization of monoclinic phases. On the other hand, flexoelectric coupling with rotostriction effect may further enrich the behavior in the $Eu_xSr_{1-x}TiO_3$ solid solution systems. It was theoretically shown that flexoelectric coupling combined with a rotostriction effect can lead to a spontaneous polarization within ferroelastic twin walls[30] and the wall-surface junctions.[36] The predicted interfacial ferroelectric phase was recently validated by experimental measurements[37] of domain-wall damping and elastic softening of twin walls in $SrTiO_3$.

Here, we study the long-range structural and polar ordering as well as the phase diagrams of $Eu_xSr_{1-x}TiO_3$ thin, strained films using LGD theory and phase-field modeling. We focus on the origin of a low-symmetry ferroelectric monoclinic phase, the stability of which is found to be related to the Eu content and the flexoroto coupling that appears at the twin walls. This paper is organized as follows: The LGD potential for $Eu_xSr_{1-x}TiO_3$ is presented in Sec. II. Phase diagrams, structural and polar properties of $Eu_xSr_{1-x}TiO_3$ thin films are analyzed in Sec. III. Flexoroto effects at elastic twin walls are studied in Sec. IV. Results are summarized in Sec. V. Material parameters of $Eu_xSr_{1-x}TiO_3$ and calculation details are given in the Supplemental Material.[45]

 ©2013 American Physical Society

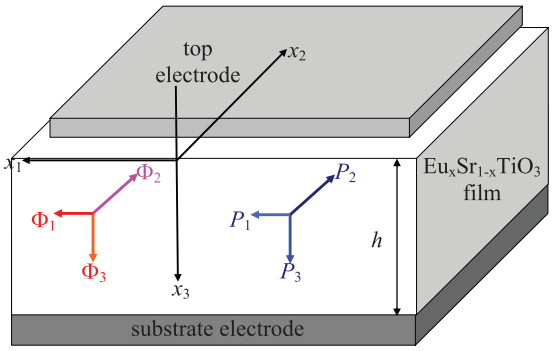

FIG. 1. (Color online) Schematics of a short-circuited $Eu_xSr_{1-x}TiO_3$ film clamped on a rigid substrate.

II. LGD POTENTIAL FOR $Eu_xSr_{1-x}TiO_3$

Let us consider a short-circuited $Eu_xSr_{1-x}TiO_3$ film of thickness h that is clamped onto a rigid substrate (Fig. 1). The lattice mismatch between the film and substrate leads to an in-plane strains u_m at the interface. Following Pertsev *et al.*,[33] the misfit strain can be calculated as $u_m = (b - a_0)/b$, where b is the substrate lattice parameter and a_0 is the cell constant of the free-standing film extrapolated from a cubic phase.

AFD structural order is characterized by the spontaneous displacement of oxygen atoms that can also be viewed as oxygen octahedron rotation (measured as displacement of oxygen ion or "tilts"), described by an axial vector Φ_i ($i = 1, 2, 3$).[29] Polarization is described by vector P_i. In this article, we only focus on the polar structural subsystem at temperatures higher than 50 K. Magnetic properties of $EuTiO_3$ at lower temperatures have been discussed elsewhere.[24–26,38]

Gibbs potential density of the $Eu_xSr_{1-x}TiO_3$ solid solution as a function of polarization and oxygen octahedra tilt vectors is written as[28]

$$G = G_S + \int_0^h (G_{\text{grad}} + G_{\text{flexo}} + G_{\text{elastic}} + G_{P\Phi})dx_3, \tag{1}$$

where $G_S = a_i^S(P_i^2(0) + P_i^2(h)) + b_i^S(\Phi_i^2(0) + \Phi_i^2(h))$ is the surface contribution, $G_{\text{grad}} = \frac{g_{ijkl}}{2}(\frac{\partial P_i}{\partial x_j}\frac{\partial P_k}{\partial x_l}) + \frac{v_{ijkl}}{2}(\frac{\partial \Phi_i}{\partial x_j}\frac{\partial \Phi_k}{\partial x_l})$ is the gradient term, and $G_{\text{flexo}} = \frac{F_{ijkl}}{2}(\sigma_{ij}\frac{\partial P_k}{\partial x_l} - P_k\frac{\partial \sigma_{ij}}{\partial x_l})$ is the flexoelectric term. F_{ijkl} is the fourth-rank tensor of flexoelectric coupling that was determined experimentally for $SrTiO_3$ in a wide temperature range by Zubko *et al.*[39] G_{elastic} is the elastic contribution, and $G_{P\Phi}$ is the polarization and tilt-dependent term. The form of $G_{\text{grad}} + G_S$ is the same as listed in Ref. 38. The elastic contribution is $G_{\text{elastic}} = -s_{ijkl}\sigma_{ij}\sigma_{kl}/2$, where $s_{ijkl}(x) = x s_{ijkl}^{EuTiO_3} + (1-x)\, s_{ijkl}^{SrTiO_3}$ are elastic compliances and σ_{ij} is the elastic stress tensor. The polarization and structural parts of the second to fourth power Landau-potential density for the cubic $m3m$ parent phase is[28]

$$G_{P\Phi} = \Big(\alpha_P P_i^2 + \beta_{Pij} P_i^2 P_j^2 - Q_{ijkl}\sigma_{ij} P_k P_l + \alpha_\Phi \Phi_i^2 + \beta_{\Phi ij}\Phi_i^2\Phi_j^2 - R_{ijkl}\sigma_{ij}\Phi_k\Phi_l + \frac{\xi_{ik}}{2}\Phi_i^2 P_k^2\Big). \tag{2}$$

The biquadratic coupling between the structural order parameter Φ_i and polarization components P_i is regarded as Houchmandazeh–Laizerowicz–Salje coupling, which is defined by the tensor ξ_{ik}.[11,40,41] This coupling was considered as the reason for the appearance of magnetization inside a ferromagnetic domain wall in a nonferromagnetic media.[42] Both biquadratic coupling tensor and higher-order expansion coefficients are regarded as composition dependent, i.e., $\beta_{P,\Phi}(x) = x\beta_{p,\Phi}^{EuTiO_3} + (1-x)\,\beta_{p,\Phi}^{SrTiO_3}$ and $\xi_{ij}(x) = x\xi_{ij}^{EuTiO_3} + (1-x)\,\xi_{ij}^{SrTiO_3}$. $Q_{ijkl}(x) = x\,Q_{ijkl}^{EuTiO_3} + (1-x)\,Q_{ijkl}^{SrTiO_3}$ and $R_{ijkl}(x) = x\,R_{ijkl}^{EuTiO_3} + (1-x)\,R_{ijkl}^{SrTiO_3}$ are the electrostriction and rotostriction tensors components, respectively, which are also assumed to depend linearly on the composition x. Coefficient $\alpha_P(T,x)$ depends on the temperature T in accordance with Barrett law[43] and composition x of the $Eu_xSr_{1-x}TiO_3$ solid solution as

$$\alpha_P(T,x) = x\alpha_P^{EuTiO_3}(T) + (1-x)\,\alpha_P^{SrTiO_3}(T), \tag{3a}$$

$$\alpha_P(T) = \alpha_T^{(P)}\big(T_q^{(P)}/2\big)\Big(\coth\big(T_q^{(P)}/2T\big) - \coth\big(T_q^{(P)}/2T_c^{(P)}\big)\Big). \tag{3b}$$

Temperature $T_q^{(P)}$ is the so-called quantum vibration temperature for $SrTiO_3$ and $EuTiO_3$, which is related to polar modes. Temperature $T_c^{(P)}$ is the "effective" Curie temperature corresponding to polar soft modes in bulk $EuTiO_3$ and $SrTiO_3$.

The nonlinear composition dependence of the transition temperature between the cubic non-AFD and tetragonal AFD phases, which was experimentally measured by Guguchia *et al.*,[27] is included in Eq. (3b) as $T_S(x) \approx 113.33 + 390.84x - 621.21x^2 + 398.87x^3$.[44] To account for the experiment and Barrett law, the dependence of coefficient $\alpha_\Phi(T,x)$ on the temperature and composition x of the $Eu_xSr_{1-x}TiO_3$ solid solution is written as

$$\alpha_\Phi(T,x) = \alpha_T^{(\Phi)}(x)\big(T_q^{(\Phi)}(x)/2\big)\Big(\coth\big(T_q^{(\Phi)}(x)/2T\big) - \coth\big(T_q^{(\Phi)}(x)/2T_S(x)\big)\Big). \tag{4}$$

To determine other parameters in Eq. (4), we used linear extrapolations, e.g., $\alpha_T^{(\Phi)}(x) = x\cdot\alpha_{T\Phi}^{EuTiO_3} + (1-x)\,\alpha_{T\Phi}^{SrTiO_3}$ and $T_q^{(\Phi)}(x) = x\cdot T_{q\Phi}^{EuTiO_3} + (1-x)\,T_{q\Phi}^{SrTiO_3}$.

Gibbs potential coefficients are renormalized by the surface tension,[28,38] misfit strains,[33] and biquadratic coupling between the structural and polar-order parameters.[30,32–38] The renormalization details are listed in Appendix A, Supplemental Material.[45] The material parameters are listed in Table S1, Supplemental Material.[45] To neglect surface gradient effects in the numerical calculations, we assume that extrapolation lengths are much greater than the film thickness h. To account for possible dislocations, effective misfit strain[46] can be introduced as $u_m^*(h) = u_m$ at $h_d < h$ and $u_m^*(h) = u_m h_d/h$ at $h_d \geqslant h$, where h_d is the critical thickness for dislocation formation.

III. PHASE DIAGRAMS OF $Eu_xSr_{1-x}TiO_3$ THIN FILMS: NEW PHASES

Numerical calculations of the $Eu_xSr_{1-x}TiO_3$ thin film polar and structural properties and phase diagrams were performed as a function of temperature T, composition x, and misfit

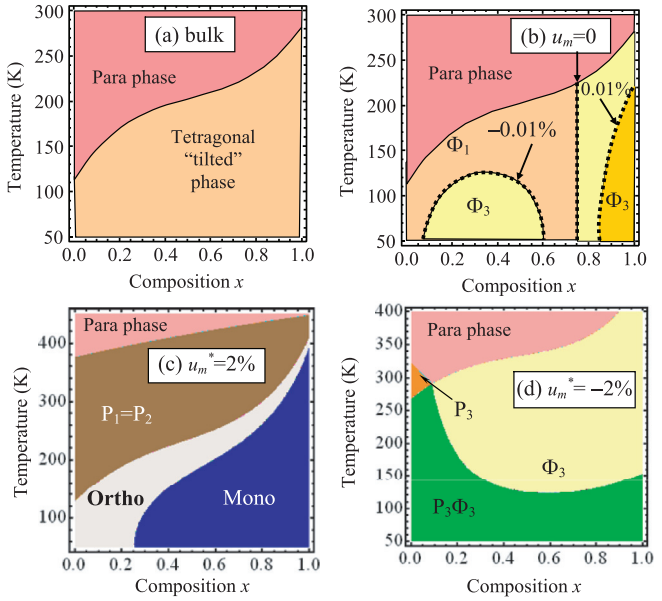

FIG. 2. (Color online) Temperature-composition phase diagrams of $Eu_xSr_{1-x}TiO_3$ bulk (a) and thin films (b)–(d). Plot (b) is calculated for the matched substrate corresponding to zero misfit $u_m = 0$ (vertical boundary Φ_1/Φ_3), $u_m^* = -0.01\%$ (left Φ_3 region), and $u_m^* = +0.01\%$ (right Φ_3 region). Plots (c)–(d) correspond to misfits $u_m^* = +2\%$ (c) and $u_m^* = -2\%$ (d).

strain u_m^*. The phase diagrams of $Eu_xSr_{1-x}TiO_3$ bulk and thin films are presented in Figs. 2–4. It should be noted that the gradient effects, which may appear in the vicinity of surfaces and domain boundaries, are ignored here for the calculation of homogeneous $Eu_xSr_{1-x}TiO_3$ films. For the same reason, poorly known polarization and tilt gradient coefficients as well as the flexoelectric effect tensor of $EuTiO_3$ are not included.

Designation $P_i\Phi_j$ in Figs. 2–4 represents the nonzero components of order parameters in a given phase. For instance $P_3\Phi_3$ corresponds to the tetragonal phase with $P_3 \neq 0$ and $\Phi_3 \neq 0$. The abbreviation "ortho" stands for the orthorhombic phase with $P_1 = P_2 \neq 0$ and $\Phi_1 = \Phi_2 \neq 0$. The abbreviation "mono" stands for the low-symmetry monoclinic phase with $P_1 \neq P_2 \neq 0$ and $\Phi_1 = \Phi_2 \neq 0$. The abbreviation "para" stands for the paraelectric nonferrodistortive phase. The boundary between AFD phases Φ_1 and Φ_3 is indicated by a thick dashed line.

The temperature-composition phase diagrams of $Eu_xSr_{1-x}TiO_3$ bulk, unstrained ($u_m = 0$), weakly strained ($|u_m| \leqslant 0.01\%$), and strongly strained ($|u_m| = 2\%$) thin films are shown in Figs. 2(a)–2(d), respectively. Two features were observed in these phase diagrams, namely, a morphotropic-like boundary between AFD in-plane and out-of-plane phases and a thermodynamically stable ferroelectric monoclinic phase.

The boundary between AFD phases Φ_1 and Φ_3 in the weakly strained films only, i.e., at $|u_m| \leqslant 0.01\%$, is morphotropic-like, and the film becomes spontaneously twinned. Note that the phases Φ_1 and Φ_3 are indistinguishable in the bulk since they are essentially the two variants of the tetragonal phase that are energetically equivalent. However, biaxial stresses exist in the thin epitaxial films clamped to a rigid substrate even at the zero misfit strain (see Appendix A,

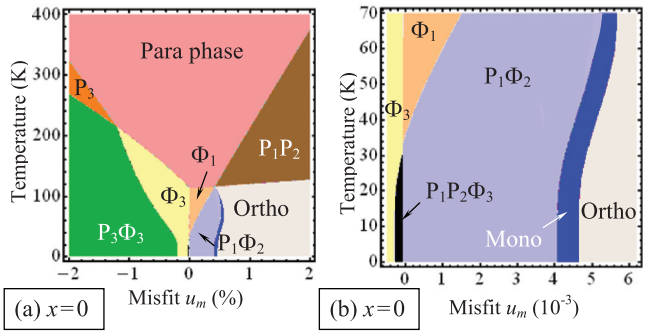

FIG. 3. (Color online) Temperature-misfit strain phase diagrams of $SrTiO_3$ thin films for a wide range of misfit strain (a) and for its small values (b).

Supplemental Material[45]). However, the biaxial stress leads to the renormalization of the coefficients β_{Pij}^* and $\beta_{\Phi ij}^*$. Since $\alpha_{\Phi i}^* = \alpha_{\Phi i}$ at $u_m = 0$ according to Eq. (2), the symmetry between the in-plane and out-of-plane directions is broken. Thus, the AFD phases with the order parameter pointed along these two directions become thermodynamically nonequivalent.

$Eu_xSr_{1-x}TiO_3$ films phase diagrams are mainly inline with the earlier theoretical calculations for $SrTiO_3$[7,12] and experiment,[47] as well as for $EuTiO_3$ *ab initio* calculations[24] and experiments.[25,26] It is well-known that tensile strains induce in-plane ferroelectric polarization in both $SrTiO_3$[7,12] and $EuTiO_3$.[24,25] Several theoretical studies[7,12] predicted that compressive strains can induce out-of-plane tetragonal ferroelectric phase in $SrTiO_3$. Jang *et al.* confirmed the ferroelectricity in $SrTiO_3$ films on a (110) $NdGaO_3$ substrate

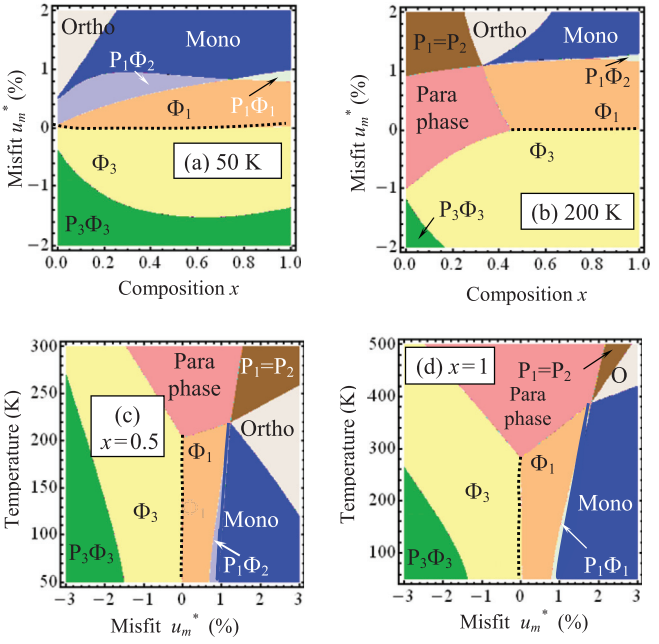

FIG. 4. (Color online) The misfit strain-composition phase diagrams of $Eu_xSr_{1-x}TiO_3$ thin films at temperature 50 K (a) and 200 K (b). Temperature-misfit strain phase diagrams of the films of composition $x = 0.5$ (c) and $x = 1$ (d).

with an average biaxial compressive strain of -1.18% under a fully commensurate condition. The absence of ferroelectricity in $SrTiO_3$ films grown on compressive (La,Sr)(Al,Ta)O_3 substrates, the lattice constant of which is close to that of $NdGaO_3$, may be related to the increase of AFD transition temperature.[48] Different polar properties of $SrTiO_3$/(La,Sr)(Al,Ta)O_3 and $SrTiO_3/NdGaO_3$ may originate from the strong structural anisotropy of orthorhombic $NdGaO_3$ in comparison with cubic (La,Sr)(Al,Ta)O_3 substrates.

Despite the agreement with the phenomenological studies,[7,12] we have found one important difference in $SrTiO_3$ thin films. In particular, Pertsev *et al.*[7] predicted the existence of both pure AFD phases and AFD-FE phases in homogeneous epitaxial $SrTiO_3$ films (see Fig. 1 in the paper). However, they did not report any monoclinic phases. From our calculations, an ultrathin monoclinic region of the low-symmetry monoclinic phase appears at tensile strains more than 1% for pure $SrTiO_3$ [see Figs. 3(a) and 3(b)].

The appearance of the monoclinic phase in $SrTiO_3$ and $Eu_xSr_{1-x}TiO_3$ may, at first glance, seem contradictory to the Vanderbilt and Cohen result.[49] According to them, a monoclinic phase can be thermodynamically stable only when the corresponding Landau expansion includes terms of the eighth order or higher in polarization, while our Gibbs potential only includes second and fourth-order terms. However, there are key differences between the thermodynamic conditions considered in the work by Vanderbilt and Cohen and in this work. First of all, Vanderbilt and Cohen considered a homogenous single-domain state under a stress-free condition, while we consider a thin film under a biaxial strain. Second, Vanderbilt and Cohen arrived at their conclusion by analyzing the dependence of the Landau free energy on the orientation of a three-component vector order parameter with a fixed magnitude, while we minimize the free energy of a strained film with respect to both the directions and magnitudes of two order parameters, namely, polarization and rotation, i.e., a total of six components. Therefore, our results reported here are not contradictory to those of Vanderbilt and Cohen.

Minimization of the free energy (A4) with respect to P_i and Φ_i leads to a system of six coupled cubic equations (A8) in the case of homogeneous film.[45] We derived the analytical expressions for the order parameters in the monoclinic phase with polarization components $P_1 \neq P_2 \neq 0$ and tilts $\Phi_1 \neq \Phi_2 \neq 0$ (Appendix B, Supplemental Material[45]). The degree of "monoclinity" was calculated analytically as

$$P_1^2 - P_2^2 = a_m\sqrt{\frac{P_m^4 - \phi^2\Phi_m^4}{a_m^2 - \phi^2}}, \quad \Phi_1^2 - \Phi_2^2 = \sqrt{\frac{P_m^4 - \phi^2\Phi_m^4}{a_m^2 - \phi^2}}, \tag{5}$$

where $P_m \equiv \sqrt{P_1^2 + P_2^2}$ and $\Phi_m \equiv \sqrt{\Phi_1^2 + \Phi_2^2}$. Evident expressions for a_m, ϕ^2, Φ_m and P_m are given in Appendix B, Supplemental Material.[45]

The stability of monoclinic phase (i.e., its minimal energy) was examined by the minimization of the $Eu_xSr_{1-x}TiO_3$ free energy (A4) with respect to P_1, P_2 and Φ_1, Φ_2 without any additional assumptions. The reason why the monoclinic phase is ignored by previous studies might be the assumption that $|P_1| = |P_2|$ and/or $|\Phi_1| = |\Phi_2|$. Initially, we tried to use the assumption but found the region on the phase diagram with nonphysical negative dielectric susceptibility, which indicates the instability. Furthermore, our numerical calculations indeed showed that the monoclinic phase with $|P_1| \neq |P_2| \neq 0$ and $|\Phi_1| \neq |\Phi_2| \neq 0$ is thermodynamically stable in the region.

One can see from Fig. 4 that the monoclinic phase region is strongly dependent on Eu content x and temperature. Figures 4(a)–4(d) show phase diagrams of $Eu_xSr_{1-x}TiO_3$ thin films in the coordinates of misfit strain-composition [Figs. 4(a) and 4(b)] and temperature-misfit strain [Figs. 4(c) and 4(d)]. The boundary Φ_1/Φ_3 occurs at very small misfit strains $|u_m| \leqslant 0.01\%$ and is almost independent of composition until the transition from the AFD to "para" phase takes place. The "para" phase region increases with temperature [compare Figs. 4(a) and 4(b)]. Different orthorhombic phases ($P_1 = P_2 \neq 0$ and $\Phi_1 = \Phi_2 \neq 0$ and $P_1 = P_2 \neq 0$) dominate at small x. As x increases, the monoclinic phase replaces the orthorhombic phase region. The monoclinic phase exists in tensile strained $EuTiO_3$ films ($u_m \approx 2\%$) up to temperatures 400 K and higher.

Note that at a particular composition, the free energy is a function of temperature, biaxial strain, and six order parameter components, and hence the multiphase (four to five) junctions in the phase diagrams in Figs. 3(a) and 4 are thermodynamically possible. The Gibbs phase rule is violated as not applicable for the case.[50] Existing publications have also shown such multiphase junctions, e.g., five phases can meet in one point in the $SrTiO_3$ phase diagram.[7,51]

One can see from Figs. 5(a) and 5(b) that the linear dielectric permittivity demonstrates typical peculiarities (jump or divergences) near the phase transitions. The nonzero component of the permittivity tensor ε_{12} and the condition $\varepsilon_{11} \neq \varepsilon_{22} \neq \varepsilon_{33}$ are the unique features of the monoclinic phase realization in the tensile-strained $Eu_xSr_{1-x}TiO_3$ films. The dielectric anisotropy factors $\varepsilon_{11}/\varepsilon_{22}$ and $\varepsilon_{22}/\varepsilon_{33}$ range from several to several hundreds of times for the $Eu_{0.5}Sr_{0.5}TiO_3$ films with effective misfit strain $u_m{}^* = +1\%$, meaning the monoclinicity can strongly affect the anisotropy of dielectric permittivity. Temperature dependence of piezoelectric constants in the monoclinic phase ($0 < T < 380$ K) of tensile-strained $EuTiO_3$ film is shown in Fig. 5(c). The values characterize the piezoelectric response of a single-domain film. Some components of piezoelectric response are drastically enhanced in the vicinity of the twin walls [Fig. 5(d)], indicating the possible appearance of new highly tunable states in incipient ferroelectrics.

Note that the temperature dependence of dielectric permittivity of $Eu_{0.5}Sr_{0.5}TiO_3$ shown in Figs. 5(a)–5(c) is calculated for the homogeneous films without gradient effects and thus does not require information about polarization, tilt gradient coefficients, and the flexoelectric effect tensor of $EuTiO_3$, which are currently unknown. The quantitative validity of the profiles of piezoelectric response components calculated across the twin walls and shown in Fig. 5(d) is under question because we used the gradient and flexoelectric coefficients of $SrTiO_3$ to generate the curves. However, we believe that Fig. 5(d) is at least qualitatively correct because the values of flexoelectric coefficients measured experimentally for $SrTiO_3$ by Zubko *et al.*[39] are in a reasonable agreement with microscopic theoretical estimations made by Kogan,[52] as well as with recent density functional theory calculations for other ferroelectric perovskites.[53,54] In other words, one can

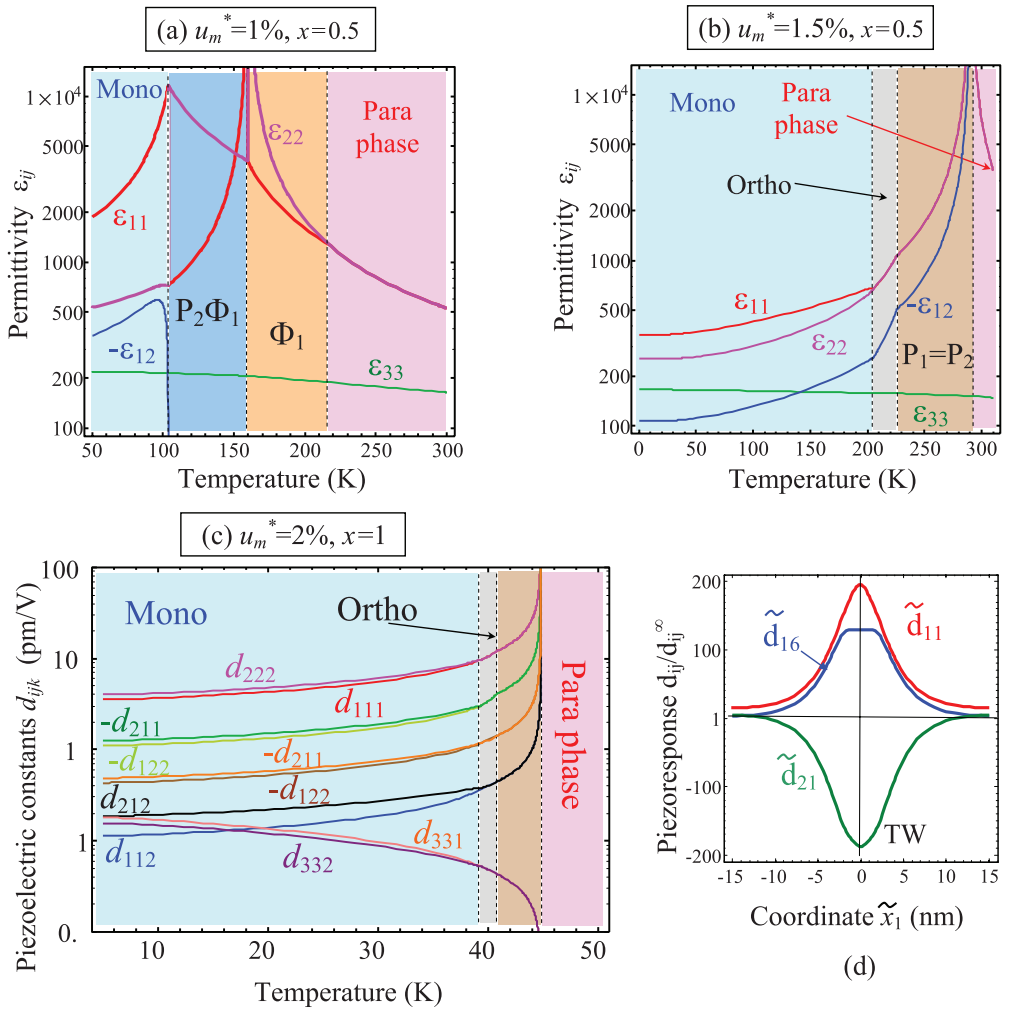

FIG. 5. (Color online) Temperature dependence of dielectric permittivity of $Eu_{0.5}Sr_{0.5}TiO_3$ films calculated for tensile misfit strains $u_m^* = +1\%$ (a), $u_m^* = +1.5\%$ (b). Temperature dependence of piezoelectric constants of tensiled $EuTiO_3$ film, $u_m^* = +2\%$ (c). Different phases are separated by the vertical lines. Phase designations are the same as in Fig. 4. Schematic profiles of several piezoelectric response components across the twin walls (d).

expect that the flexoelectric tensor should not differ much for perovskites $SrTiO_3$ and $EuTiO_3$.

Our calculations show that the favorable condition of the monoclinic phase appearance in $Eu_xSr_{1-x}TiO_3$ is the *negative sign* of biquadratic coupling tensor coefficients ξ_{ik} (see Table I). Also LGD expansion coefficients α^*_{Pi} and $\alpha^*_{\Phi i}$ should be negative, but these conditions could be readily reached in the strained films since the coefficients are essentially renormalized by misfit strains. The conditions $\xi^*_{ij} < 0$ are valid if $\xi_{ij} < 0$, because the renormalization of ξ_{ik} by misfit effect is usually small. The opposite signs of the coupling tensor ξ_{ik} in $SrTiO_3$ and $EuTiO_3$ can explain the increase of the monoclinic phase region with the increase of Eu content, x. Thus, we can conclude that the simultaneous presence of both octahedra tilts and polarization in epitaxial $Eu_xSr_{1-x}TiO_3$ films stabilizes the in-plane monoclinic phase at moderate and high tensile strains $u_m > 1\%$.

TABLE I. Biquadratic coupling type with respect to the monoclinic phase origin.

AFD material	Biquadratic coupling type	Refs.
$SrTiO_3$	Unfavorable	e.g.[7]
$EuTiO_3$	Favorable	Our fit
$CaTiO_3$	Unfavorable	Gu *et al.*[5]
$PbZr_xTi_{1-x}O_3$	Favorable	Haun *et al.*[40]

It should be noted that the monoclinic phase can also appear as the intermediate phase between the phases with higher-order symmetry.[55] For example, the monoclinic phase was found in $Pb(Zr,Ti)O_3$ by Noheda *et al.*[56] at the morphotropic boundary between tetragonal and rhombohedral phases. It was demonstrated[57] that the monoclinic phase in $Pb(Zr,Ti)O_3$ is accompanied by the octahedral tilts, at least at lower temperatures. Local inhomogeneity can stabilize monoclinic phase as well. The monoclinic phase was predicted in the superlattices $BaTiO_3/SrTiO_3$[58] as a consequence of complex electrostatic and elastic interactions within an inhomogeneous domain structure in the multilayered ferroelectric film.

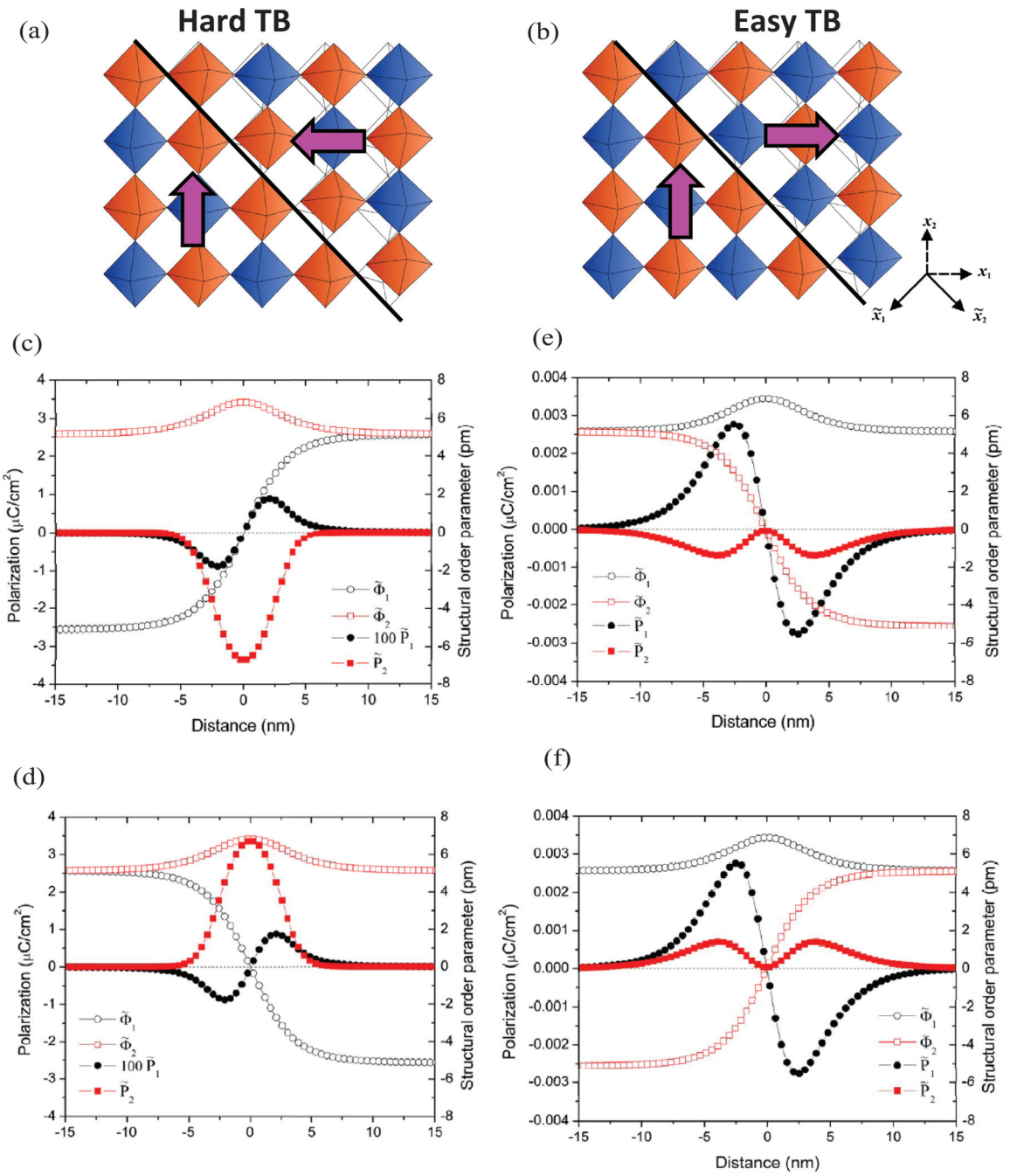

FIG. 6. (Color online) (a) Configuration of oxygen octahedral tilt across the "head-to-head" hard TB. (b) Configuration of oxygen octahedral tilt across the "head-to-tail" easy TB. (c)–(f) The spontaneous polarization induced by the tilt gradient in the vicinity of the TB. Results are calculated by the phase-field modeling for $SrTiO_3$ parameters.

IV. FLEXOROTO EFFECTS AT ELASTIC TWINS IN $Eu_xSr_{1-x}TiO_3$

The monoclinic phase is characterized by the high number of energetically equivalent tilt and polarization domain variants, leading to no less than 16 types of twins, consisting of eight ferroelectric twin pairs with different orientations of tilt vector. The high number of possible domain pairs (mostly twins) results in easy twinning of a strained film and consequently enhance the piezoelectric response and electromechanical tunability.

The film becomes spontaneously twinned in the vicinity of morphotropic boundaries Φ_1/Φ_3 as well as in the monoclinic phase with $P_1 \neq P_2 \neq 0$ and $\Phi_1 \neq \Phi_2 \neq 0$. Due to the presence of rotostriction and flexoelectric coupling, spontaneous polarization and piezo- and pyroelectricity may arise from elastic twin boundaries (TB).[30] Recent experimental measurements[37] seem to confirm these theoretical predictions. For example, Scott *et al.*[37] studied the damping and elastic softening of twin walls in bulk $SrTiO_3$ and showed that ferroelastic domain walls become ferroelectric at low temperatures.

The joint action of rotostriction and flexoelectric coupling[30] produces the inhomogeneous strain $u_{ij}(\mathbf{r}) \propto R_{mnpq}\,\partial(\Phi_p\Phi_q)/\partial x_l$ across the structural TB that induces the variation of polarization ($\delta P_i(\mathbf{r})$), piezoelectric ($\delta d_{ijk}(\mathbf{r})$), and pyroelectric ($\delta\Pi_i(\mathbf{r})$) responses as

$$\delta P_i(\mathbf{r}) \propto -\alpha_{iv}^{-1} f_{mnvl} R_{mnpq} \frac{\partial(\Phi_p\Phi_q)}{\partial x_l}, \tag{6a}$$

$$\delta d_{ijk}(\mathbf{r}) \approx 2\varepsilon_0\varepsilon_{im} Q_{mkjl}\delta P_l(\mathbf{r}),$$
$$\delta\Pi_i(\mathbf{r}) = -\gamma_{ij}\frac{\partial}{\partial T}\delta P_j(\mathbf{r}), \tag{6b}$$

where f_{mnvl} denotes direct flexoelectric tensor, $f_{ijkl} = c_{ijmn}F_{mnkl}$, γ_{ij} is the pyroelectric coefficients tensor, $\varepsilon_0 = 8.85\times10^{-12}$ F/m is the universal dielectric constant, and ε_{ij} is the relative dielectric permittivity. Note that Eq. (6a) is valid only for the zero electric field, including both external and depolarization fields. Estimations based in Eq. (6) give 0.5−5 C/m^2 for $\delta P_i(\mathbf{r})$, 10 pm/V for $\delta d_{ijk}(\mathbf{r})$, and (5−50) 10^{-6} C/m^{2}K for $\delta\Pi_i(\mathbf{r})$, depending on temperature and content x. The numerical values are in agreement with previous studies of roto-flexo effect.[30–32] Note that there are other possible reasons for polar surface states in nonpolar materials such as $SrTiO_3$, e.g., surface piezoelectricity.[59–62] For example, Dai *et al.*[62] obtained surface polarization ∼(0.07–0.02) μC/cm^2 for $SrTiO_3$ in a wide temperature range. However, the roto-flexo effect can lead to higher polarization values ∼(0.5–5) μC/cm^2 in the AFD phase.

The spontaneous polarization induced by the tilt gradient in the vicinity of $SrTiO_3$ TB was obtained by the phase-field modeling. Profiles of the tilts $\tilde{\Phi}_1$ and $\tilde{\Phi}_2$ and polarization $\tilde{P}_1$ and $\tilde{P}_2$ components calculated across the easy and hard TB are presented in Fig. 6. The calculations were performed in the rotated frame $\{\tilde{x}_1,\tilde{x}_2\}$ shown in Fig. 6(b). For hard TB, $\tilde{P}_1$ is odd, and $\tilde{P}_2$ is even [see Figs. 6(c) and 6(d)]. The even Bloch-type component $\tilde{P}_2$ flips when $\tilde{\Phi}_1$ flips, as one can conclude comparing the Figs. 6(c) and 6(d). The magnitude of $\tilde{P}_1$ and $\tilde{P}_2$ are quite different, and this is similar to the hard antiphase boundaries.[30] For easy TB $\tilde{P}_1$ is odd and $\tilde{P}_2$ is even [see Figs. 6(e) and 6(f)]. The even $\tilde{P}_2$ flips when $\tilde{\Phi}_2$ flips, as one can see comparing the Figs. 6(e) and 6(f). The magnitudes of $\tilde{P}_1$ and $\tilde{P}_2$ are similar. These results are in semiquantitative agreement with previous analytical results.[30] However, one interesting parity-related effect that was not reported previously is evident. It is the flip of the even Bloch-type polarization distribution $\tilde{P}_2$ with the sign change of the Ising-type tilt component $\tilde{\Phi}_1$. At the same time, the odd component of polarization profile is independent of the tilt sign. The result can be explained by analyzing the symmetry of the inhomogeneous strains $\tilde{u}_{ij}(\mathbf{r}) \propto \tilde{R}_{mnpq}\,\partial(\tilde{\Phi}_p\tilde{\Phi}_q)/\partial\tilde{x}_l$, which are responsible for the appearance of components $\tilde{P}_1$ and $\tilde{P}_2$ in the vicinity of TB. The origin for the polarization components are $\tilde{P}_1 \propto \partial(\tilde{\Phi}_1^2)/\partial\tilde{x}_1$ and $\tilde{P}_2 \propto \partial(\tilde{\Phi}_1\tilde{\Phi}_2)/\partial\tilde{x}_1$ according to the Euler–Lagrange equations.[30] Therefore, $\tilde{P}_1$ is the even function of $\tilde{\Phi}_1$, and $\tilde{P}_2$ is the odd function of $\tilde{\Phi}_1$.

Note that there were misprints in the gradient coefficients in Ref. 5. The corrected set of $SrTiO_3$ coefficients is given in the Table S1, Supplemental Material.[63] Using the set of parameters from Table S1, Supplemental Material,[45] we found that two kinds of TB have similar wall width (compare left and right column in Fig. 6).

V. SUMMARY

Using LGD second to fourth power expansion and phase-field modeling, we studied the interplay between the long-range structural order parameter and polarization in epitaxial $Eu_xSr_{1-x}TiO_3$ thin films.

A new low-symmetry ferroelectric monoclinic phase is shown to become stable in $Eu_xSr_{1-x}TiO_3$ thin films at moderate tensile strains. We derived analytical expressions for the spontaneous tilt and ferroelectric polarization vectors for the monoclinic phase and demonstrated that the presence of AFD octahedra tilts stabilizes the monoclinic phase with in-plane ferroelectric polarization. The monoclinic phase region is strongly dependent on the Eu content. It is also shown that the monoclinic phase is thermodynamically stable in a wide temperature range. The monoclinic phase is characterized by a large number of energetically equivalent orientations of the polar and structural order parameters. Since the local elastic field gradients of adjacent domain walls will interact, the appearance of highly tunable piezoelectricity in the incipient ferroelectric films is possible, while it is not expected in the corresponding bulk $Eu_xSr_{1-x}TiO_3$.

Using phase-field modeling, we demonstrate that the flexoelectric coupling and rotostriction give rise to the spontaneous polarization at the elastic TB due to the intrinsic strain gradient. The interfacial polarization displays an interesting parity-related effect, namely, changing the sign of the Ising-type tilt component leads to the flip of the Bloch-type polarization distribution.

ACKNOWLEDGMENTS

A.N.M., M.D.G., V.V.K, and E.A.E. acknowledge the State Fund for Fundamental Research of Ukraine, SFFR-NSF Grant No. UU48/002. Y.G, V.G., and L.Q.C. acknowledge the financial support by the U.S. National Science Foundation under NSF-DMR-0908718, NSF-DMR-0820404, and NSF-DMR-1210588.

*lqc3@ems.psu.edu
†vxg8@psu.edu
‡eugene.a.eliseev@gmail.com

[1] D. G. Schlom, L.-Q. Chen, C.-B. Eom, K. M. Rabe, S. K. Streiffer, and Jean-Marc Triscone, Annu. Rev. Mater. Res. **37**, 589 (2007).
[2] D. D. Fong, G. B. Stephenson, S. K. Streiffer, J. A. Eastman, O. Auciello, P. H. Fuoss, and C. Thompson, Science **304**, 1650 (2004).
[3] M. J. Highland, T. T. Fister, D. D. Fong, P. H. Fuoss, C. Thompson, J. A. Eastman, S. K. Streiffer, and G. B. Stephenson, Phys. Rev. Lett. **107**, 187602 (2011).

[4]Y.-H. Chu, L. W. Martin, M. B. Holcomb, M. Gajek, S.-J. Han, Q. He, N. Balke, C.-H. Yang, D. Lee, W. Hu, Q. Zhan, P.-L. Yang, A. Fraile-Rodríguez, A. Scholl, S. X. Wang, and R. Ramesh, Nat. Mater. **7**, 478 (2008).
[5]Y. Gu, K. Rabe, E. Bousquet, V. Gopalan, and L.-Q. Chen, Phys. Rev. B **85**, 064117 (2012).
[6]Y. Yang, W. Ren, M. Stengel, X. H. Yan, and L. Bellaiche, Phys. Rev. Lett. **109**, 057602 (2012).
[7]N. A. Pertsev, A. K. Tagantsev, and N. Setter, Phys. Rev. B **61**, R825 (2000).
[8]W. Cao and G. R. Barsch, Phys. Rev. B **41**, 4334 (1990).
[9]P. A. Fleury, J. F. Scott, and J. M. Worlock, Phys. Rev. Lett. **21**, 16 (1968).
[10]P. A. Fleury and J. M. Worlock, Phys. Rev. **174**, 613 (1968).
[11]A. K. Tagantsev, E. Courtens, and L. Arzel, Phys. Rev. B **64**, 224107 (2001).
[12]J. H. Haeni, P. Irvin, W. Chang, R. Uecker, P. Reiche, Y. L. Li, S. Choudhury, W. Tian, M. E. Hawley, B. Craigo, A. K. Tagantsev, X. Q. Pan, S. K. Streiffer, L. Q. Chen, S. W. Kirchoefer, J. Levy, and D. G. Schlom, Nature (London) **430**, 758 (2004).
[13]Y. L. Li, S. Choudhury, J. H. Haeni, M. D. Biegalski, A. Vasudevarao, A. Sharan, H. Z. Ma, J. Levy, V. Gopalan, S. Trolier-McKinstry, D. G. Schlom, Q. X. Jia, and L. Q. Chen, Phys. Rev. B **73**, 184112 (2006).
[14]A. Ohtomo and H. Y. Hwang, Nature (London) **427**, 423 (2004).
[15]R. Oja, M. Tyunina, L. Yao, T. Pinomaa, T. Kocourek, A. Dejneka, O. Stupakov, M. Jelinek, V. Trepakov, S. van Dijken, and R. M. Nieminen, Phys. Rev. Lett. **109**, 127207 (2012).
[16]Y. Y. Guo, H. M. Liu, D. P. Yu, and J.-M. Liu, Phys. Rev. B **85**, 104108 (2012).
[17]T. Katsufuji and H. Takagi, Phys. Rev. B **64**, 054415 (2001).
[18]V. V. Shvartsman, P. Borisov, W. Kleemann, S. Kamba, and T. Katsufuji, Phys. Rev. B **81**, 064426 (2010).
[19]A. Bussmann-Holder, J. Kohler, R. K. Kremer, and J. M. Law, Phys. Rev. B **83**, 212102 (2011).
[20]M. Allieta, M. Scavini, L. J. Spalek, V. Scagnoli, H. C. Walker, C. Panagopoulos, S. S. Saxena, T. Katsufuji, and C. Mazzoli, Phys. Rev. B **85**, 184107 (2012).
[21]K. Z. Rushchanskii, N. A. Spaldin, and M. Lezaic, Phys. Rev. B **85**, 104109 (2012).
[22]V. Goian, S. Kamba, O. Pacherova, J. Drahokoupil, L. Palatinus, M. Dusek, J. Rohlıcek, M. Savinov, F. Laufek, W. Schranz, A. Fuith, M. Kachlık, K. Maca, A. Shkabko, L. Sagarna, A. Weidenkaff, and A. A. Belik, Phys. Rev. B **86**, 054112 (2012).
[23]A. P. Petrović, Y. Kato, S. S. Sunku, T. Ito, P. Sengupta, L. Spalek, M. Shimuta, T. Katsufuji, C. D. Batista, S. S. Saxena, and C. Panagopoulos, Phys. Rev. B **87**, 064103 (2013).
[24]C. J. Fennie and K. M. Rabe, Phys. Rev. Lett. **97**, 267602 (2006).
[25]J. H. Lee, L. Fang, E. Vlahos, X. Ke, Y. Woo Jung, L. F. Kourkoutis, Jong-Woo Kim, P. J. Ryan, Tassilo Heeg, M. Roeckerath, V. Goian, M. Bernhagen, R. Uecker, P. C. Hammel, K. M. Rabe, S. Kamba, J. Schubert, J. W. Freeland, D. A. Muller, C. J. Fennie, P. Schiffer, V. Gopalan, E. Johnston-Halperin, and D. Schlom, Nature (London) **466**, 954 (2010).
[26]P. J. Ryan, J.-W. Kim, T. Birol, P. Thompson, J.-H. Lee, X. Ke, P. S. Normile, E. Karapetrova, P. Schiffer, S. D. Brown, C. J. Fennie, and D. G. Schlom, Nat. Commun. **4**, 1334 (2013).
[27]Z. Guguchia, A. Shengelaya, H. Keller, J. Kohler, and A. Bussmann-Holder, Phys. Rev. B **85**, 134113 (2012).
[28]E. A. Eliseev, M. D. Glinchuk, V. V. Khist, C.-W. Lee, C. S. Deo, R. K. Behera, and A. N. Morozovska, J. Appl. Phys. **113**, 024107 (2013).
[29]V. Gopalan and D. B. Litvin, Nat. Mater. **10**, 376 (2011).
[30]A. N. Morozovska, E. A. Eliseev, M. D. Glinchuk, L.-Q. Chen, and V. Gopalan, Phys. Rev. B **85**, 094107 (2012).
[31]A. N. Morozovska, E. A. Eliseev, S. V. Kalinin, L.-Q. Chen, and V. Gopalan, Appl. Phys. Lett. **100**, 142902 (2012).
[32]A. N. Morozovska, E. A. Eliseev, S. L. Bravina, A. Y. Borisevich, and S. V. Kalinin, J. Appl. Phys. **112**, 064111 (2012).
[33]N. A. Pertsev, A. G. Zembilgotov, and A. K. Tagantsev, Phys. Rev. Lett. **80**, 1988 (1998).
[34]O. Diéguez, Silvia Tinte, A. Antons, C. Bungaro, J. B. Neaton, K. M. Rabe, and D. Vanderbilt, Phys. Rev. B **69**, 212101 (2004).
[35]Y. L. Li and L. Q. Chen, Appl. Phys. Lett. **88**, 072905 (2006).
[36]E. A. Eliseev, A. N. Morozovska, Y. Gu, A. Y. Borisevich, L.-Q. Chen, V. Gopalan, and S. V. Kalinin, Phys. Rev. B **86**, 085416 (2012).
[37]J. F. Scott, E. K. H. Salje, and M. A. Carpenter, Phys. Rev. Lett. **109**, 187601 (2012).
[38]A. N. Morozovska, M. D. Glinchuk, Rakesh K. Behera, B. Zaulychny, Chaitanya S. Deo, and E. A. Eliseev, Phys. Rev. B **84**, 205403 (2011).
[39]P. Zubko, G. Catalan, A. Buckley, P. R. L. Welche, and J. F. Scott, Phys. Rev. Lett. **99**, 167601 (2007).
[40]M. J. Haun, E. Furman, T. R. Halemane, and L. E. Cross, Ferroelectrics **99**, 55 (1989); M. J. Haun, E. Furman, S. J. Jang, and L. E. Cross, *ibid.* **99**, 13 (1989).
[41]B. Houchmanzadeh, J. Lajzerowicz, and E. Salje, J. Phys.: Condens. Matter **3**, 5163 (1991).
[42]M. Daraktchiev, G. Catalan, and J. F. Scott, Ferroelectrics **375**, 122 (2008).
[43]J. H. Barrett, Phys. Rev. **86**, 118 (1952).
[44]A. Bussmann-Holder (private communication, 2012).
[45]See Supplemental Material at http://link.aps.org/supplemental/10.1103/PhysRevB.87.134102 for calculation details.
[46]J. S. Speck and W. Pompe, J. Appl. Phys. **76**, 466 (1994).
[47]H. W. Jang, A. Kumar, S. Denev, M. D. Biegalski, P. Maksymovych, C. W. Bark, C. T. Nelson, C. M. Folkman, S. H. Baek, N. Balke, C. M. Brooks, D. A. Tenne, D. G. Schlom, L. Q. Chen, X. Q. Pan, S. V. Kalinin, V. Gopalan, and C. B. Eom, Phys. Rev. Lett. **104**, 197601 (2010).
[48]T. Yamada, T. Kiguchi, A. K. Tagantsev, H. Morioka, T. Iijima, H. Ohsumi, S. Kimura, M. Osada, N. Setter, and H. Funakubo, Integr. Ferroelectr. **115**, 57 (2010).
[49]D. Vanderbilt and M. H. Cohen, Phys. Rev. B **63**, 094108 (2001).
[50]W. C. Johnson, Metall. Trans. A **18**, 1093 (1987).
[51]N. A. Pertsev, A. K. Tagantsev, and N. Setter, Phys. Rev. B **65**, 219901(E) (2002).
[52]Sh. M. Kogan, Sov. Phys. Solid State **5**, 2069 (1964).
[53]J. Hong and D. Vanderbilt, Phys. Rev. B **84**, 180101(R) (2011).
[54]I. Ponomareva, A. K. Tagantsev, and L. Bellaiche, Phys. Rev. B **85**, 104101 (2012).

[55]M. Iwata and Y. Ishibashi, Jpn. J. Appl. Phys. **44**, 3095 (2005).
[56]B. Noheda, D. E. Cox, G. Shirane, J. A. Gonzalo, L. E. Cross, and S.-E. Park, Appl. Phys. Lett. **74**, 2059 (1999).
[57]F. Cordero, F. Trequattrini, F. Craciun, and C. Galassi, J. Phys.: Condens. Matter **23**, 415901 (2011).
[58]P. Wu, X. Ma, Y. Li, V. Gopalan, and L.-Q. Chen, Appl. Phys. Lett. **100**, 092905 (2012).
[59]N. D. Sharma, R. Maranganti, and P. Sharma, J. Mech. Phys. Solids **55**, 2328 (2007).
[60]A. Kholkin, I. Bdikin, T. Ostapchuk, and J. Petzelt, Appl. Phys. Lett. **93**, 222905 (2008).
[61]N. D. Sharma, C. M. Landis, and P. Sharma, J. Appl. Phys. **108**, 024304 (2010).
[62]S. Dai, M. Gharbi, P. Sharma, and H. S. Park, J. Appl. Phys. **110**, 104305 (2011).
[63]See Supplemental Material at http://link.aps.org/supplemental/10.1103/PhysRevB.87.134102 for a correction to the Ref. 28 coefficients.